


Article

Resonance Raman Spectroscopy of Mn-Mg_k Cation Complexes in GaN

Andrii Nikolenko ^{1,*} , Viktor Strelchuk ¹, Bogdan Tsykaniuk ¹, Dmytro Kysylychyn ², Giulia Capuzzo ² and Alberta Bonanni ²

¹ V. Lashkaryov Institute of Semiconductor Physics of National Academy of Sciences of Ukraine, 41 Nauky pr., 03028 Kyiv, Ukraine; viktor.strelchuk@ccu-semicond.net (V.S.); btsykaniuk@gmail.com (B.T.)

² Institut für Halbleiter-und-Festkörperphysik, Johannes Kepler University, Altenbergerstr. 69, A-4040 Linz, Austria; d.kysylychyn@gmail.com (D.K.); giulia.capuzzo@jku.at (G.C.); alberta.bonanni@jku.at (A.B.)

* Correspondence: nikolenko@isp.kiev.ua

Received: 15 April 2019; Accepted: 2 May 2019; Published: 4 May 2019



Abstract: Resonance Raman analysis is performed in order to gain insight into the nature of impurity-induced Raman features in GaN:(Mn,Mg) hosting Mn-Mg_k cation complexes and representing a prospective strategic material for the realization of full-nitride photonic devices emitting in the infra-red. It is found that in contrast to the case of GaN:Mn, the resonance enhancement of Mn-induced modes at sub-band excitation in Mg co-doped samples is not observed at an excitation of 2.4 eV, but shifts to lower energies, an effect explained by a resonance process involving photoionization of a hole from the donor level of Mn to the valence band of GaN. Selective excitation within the resonance Raman conditions allows the structure of the main Mn-induced phonon band at ~670 cm⁻¹ to be resolved into two distinct components, whose relative intensity varies with the Mg/Mn ratio and correlates with the concentration of different Mn-Mg_k cation complexes. Moreover, from the relative intensity of the 2LO and 1LO Raman resonances at inter-band excitation energy, the Huang-Rhys parameter has been estimated and, consequently, the strength of the electron-phonon interaction, which is found to increase linearly with the Mg/Mn ratio. Selective temperature-dependent enhancement of the high-order multiphonon peaks is due to variation in resonance conditions of exciton-mediated outgoing resonance Raman scattering by detuning the band gap.

Keywords: metal-organic vapor phase epitaxy; III-nitrides; cation complexes; resonance Raman spectroscopy; electron-phonon interaction

1. Introduction

Gallium nitride (GaN)-based semiconductors, due to their remarkable properties such as wide tunability of direct band-gap, the availability of both *n*- and *p*-type material, high thermal stability, large heat conductivity, high electric field strength, and electron mobility, are key materials for state-of-the-art high-efficiency optoelectronic devices, such as blue, ultra-violet, and white light emitting diodes (LEDs) [1], laser diodes [2], and high-power and high-frequency electronic devices, like e.g., electron mobility transistors (HEMTs) [3]. Moreover, as recently demonstrated, the co-doping of GaN with Mn and Mg results in the formation of Mn-Mg_k cation complexes—with *k* the number of ligands [4]—which are responsible for a strong room-temperature broad near infra-red (NIR) emission and open wide perspectives to extend the functionalities of III-nitride systems to the NIR range without the need of rare earths or In [5].

Raman spectroscopy is an informative tool to investigate impurities and impurity complexes in semiconductors by probing their specific impurity-induced local vibrational modes (LVM) [6,7],

which can be significantly enhanced in resonance conditions, i.e., when the energy of the excitation is close or coincides with one of the electron energy levels in the system. Doping of GaN with Mg and Mn leads to a rich set of impurity-related Raman bands. The most prominent feature related to the incorporation of Mn is the phonon band detected at 667 cm^{-1} [8,9]. This mode was shown to have a strong polarization dependence similar to the one of the $A_1(\text{LO})$ mode of GaN [9], a resonance enhancement at an excitation of 2.4 eV and a linear-like dependence on the Mn concentration [8]. The 667 cm^{-1} band, together with a set of less intense phonon bands found in the range between the E_2^{high} and the $A_1(\text{LO})$ modes of GaN at $\sim 600\text{ cm}^{-1}$, $\sim 630\text{ cm}^{-1}$, and between 700 cm^{-1} and 730 cm^{-1} , were compared with the calculated phonon density of states (DOS) of GaN:Mn and attributed to modes activated by disorder in the nitrogen sublattice, while their high intensity is explained by the impurity-induced Fröhlich type resonance Raman scattering related to the charge transfer level of the Mn^{2+} center [9]. Raman modes in Mg-doped GaN found at 136 cm^{-1} , 262 cm^{-1} , and 656 cm^{-1} were attributed to LVM modes of Mg on Ga sites, while broad bands around 320 cm^{-1} and 595 cm^{-1} originate from disorder-activated scattering [10,11]. All mentioned modes exhibit A_1 symmetry and scale with the Mg concentration.

Doping of epitaxial GaN films with Mn results in the onset of a Mn-induced feature at 667 cm^{-1} , which in the case of disordered Mn-implanted GaN structures was assigned to the LVM of GaN related to nitrogen vacancies V_N , since this mode shows a significant polarization dependence, becomes sharper with decreasing Mn content, i.e., at lower defect concentration, and is found in GaN implanted with different foreign elements [12,13]. In contrast, the phonon band at $(579\text{--}586)\text{ cm}^{-1}$ is attributed to the LVM of Mn, in view of its strong polarization dependence consistent with the local symmetry of Mn ions occupying Ga sites and of its frequency consistent with the one estimated within the light impurity model [8,13]. The broad background bands centered at 300 cm^{-1} , 430 cm^{-1} , and 730 cm^{-1} respectively—also found in ion-implanted GaN [12]—show no relevant polarization dependence and are related to a defect-induced response due to the activation of the phonon DOS [13].

The Mn-induced Raman features are significantly modified when GaN:Mn is co-doped with Mg. The behavior of the impurity-related bands in GaN:(Mn,Mg) containing Mn-Mg_k cation complexes was reported as a function of the Mg/Mn ratio [8]. In particular, it was shown that co-doping of GaN:Mn with Mg leads to: (i) a significant decay of the Mn-induced features in the range between the E_2^{high} and the $A_1(\text{LO})$ modes of GaN, and to a lesser extent, in correspondence of the 667 cm^{-1} band; (ii) a gradual high-frequency shift of the 667 cm^{-1} band with increasing Mg/Mn ratio, consistent with the shortening of the Mn-N bond length in the Mn-Mg_k cation complexes expected from ab initio calculations [4]; (iii) the appearance of a broad structure at $\sim 688\text{ cm}^{-1}$, whose intensity correlates with the presence of Mn-Mg₂ complexes.

Here, the in-depth analysis of excitation-dependent resonance Raman spectroscopy at a sub-band-gap excitation of GaN:(Mn,Mg) with Mn-Mg_k IR-emitting cation complexes is reported. In addition, a resonance Raman analysis at the inter-band excitation energy is performed in order to estimate the strength of the electron-phonon interaction from the relative intensity of the 2LO and 1LO Raman resonances.

2. Materials and Methods

The investigated samples consist of a $1\text{ }\mu\text{m}$ -thick GaN buffer layer grown on *c*-sapphire (0001), on which a 600 nm-thick layer of GaN doped with Mn and/or Mg is deposited. The samples are fabricated using metalorganic vapor phase epitaxy (MOVPE) according to a procedure previously reported [4,14]. Alternatives to *c*-sapphire as substrates for the growth of nitride compounds have been widely investigated [15,16]. Furthermore, options for buffer/nucleation layers aimed at minimizing the effects of lattice and thermal mismatch between substrate and overlayers are currently considered, and significant progress has been made in the epitaxy of III-nitrides on Si [17]. Nevertheless, *c*-sapphire is still the preferred substrate for the fabrication of nitride-based optoelectronic device structures, and accordingly, it is employed in this work.

The thickness of the various epitaxial layers has been determined on-line during the growth process by means of laser reflectometry and then confirmed using complementary high-resolution transmission electron microscopy (HRTEM) on cross-sectional specimens and x-ray diffraction (XRD) measurements, as previously reported in [4,5,8,14]. Moreover, according to the applied comprehensive protocol of structural and magnetic characterization [4,5,8,14], the Mn ions (and related complexes) are randomly and homogeneously distributed over the corresponding layers (both in-plane and in the growth direction). A sketch of the architecture of the sample is provided in Figure 1, while a list of the investigated samples is given in Table 1, together with the respective Mn content x_{Mn} , Mg concentration x_{Mg} , and Mg/Mn ratio. The concentrations of Mg and Mn reported in columns 2 and 3 of Table 1 have been obtained using secondary-ion mass spectroscopy (SIMS) analysis, while the Mg/Mn ratios are the result of extended X-ray fine structure (EXAFS) data and data analysis, according to the procedures and protocols in [4].

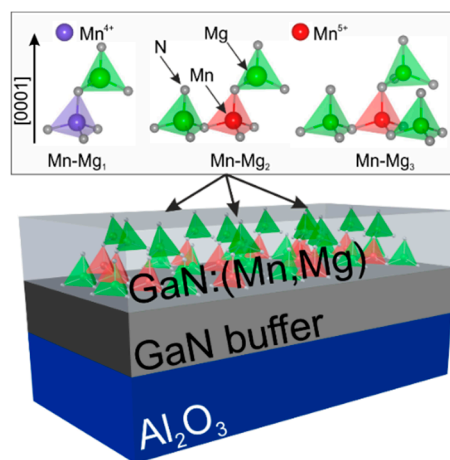


Figure 1. Schematic representation of the architecture of the samples.

Table 1. List of investigated samples, together with the respective Mn content x_{Mn} (from SIMS analysis), Mg concentration x_{Mg} (from SIMS analysis), and Mg/Mn ratio (from EXAFS measurements).

#	Sample	x_{Mn} , %	x_{Mg} , %	Mg/Mn
1	GaN:Mn	0.75	-	-
2	GaN:Mg	-	0.25	-
3	GaN:(Mn,Mg)	0.54	0.16	0.41
4	GaN:(Mn,Mg)	0.49	0.49	0.92
5	GaN:(Mn,Mg)	0.22	0.36	1.5
6	GaN:(Mn,Mg)	0.09	0.20	2.25
7	GaN:(Mn,Mg)	0.09	0.60	6.6

Room-temperature Raman spectra are collected in backscattering geometry from the c -plane at excitations of 488 nm and 514 nm using a Horiba JobinYvon T64000 micro-Raman spectrometer, at 632 nm with a Renishaw inVia micro-Raman spectrometer, and at 785 nm by means of a line-focus Raman microscope with a Princeton Instruments IsoPlane SCT-320 spectrograph [18]. Polarized Raman spectra were measured in parallel $z(y, y)\bar{z}$ and crossed $z(x, y)\bar{z}$ scattering geometries. Photoluminescence (PL) spectra were acquired at excitations of 785 nm and 514 nm, respectively.

3. Results and Discussion

3.1. Raman Spectroscopy at Sub-Band Excitation

The Raman spectra from the studied GaN:Mn, GaN:Mg, and GaN:(Mn,Mg) samples at a sub-band excitation of 2.54 eV are shown in Figure 2a and are characteristic for GaN doped with Mn and/or

was explained through a resonance process involving electron transitions from the localized level of Mn^{2+} to the conduction band and its subsequent recombination with Mn^{3+} with the emission of LO phonons [9,19]. The response was found to be significantly different for GaN:(Mn,Mg) and to vary with the ratio Mg/Mn (Figure 3b–f). The relative intensity of the impurity-induced features at the excitation of 1.58 eV gradually increases with Mg/Mn, while their intensity is quenched and the line-shape is also affected at an excitation of 2.41 eV. The vanishing of the Mn-Mg-induced vibrational features (F,C,G) upon increasing the excitation energy up to 3.82 eV is related to the deviation of the excitation from the resonance conditions. While the inter-band excitation at 3.82 eV is in resonance with the band-gap of GaN and induces a significant resonance Raman enhancement of the $A_1(\text{LO})$ phonon of the GaN matrix, it is not resonant with the charge transfer level of the Mn impurity and does not affect the Mn-Mg-induced vibrational features. This is in agreement with the previous findings by Gebicki et al. [9] for GaN:Mn, where the Mn-induced feature C is reported to reach a maximum of intensity at 2.4 eV, in resonance with the charge transfer level of Mn impurity, gradually weakening with the excitation energy, when moving away from the resonance, and fully vanishing at 3.0 eV.

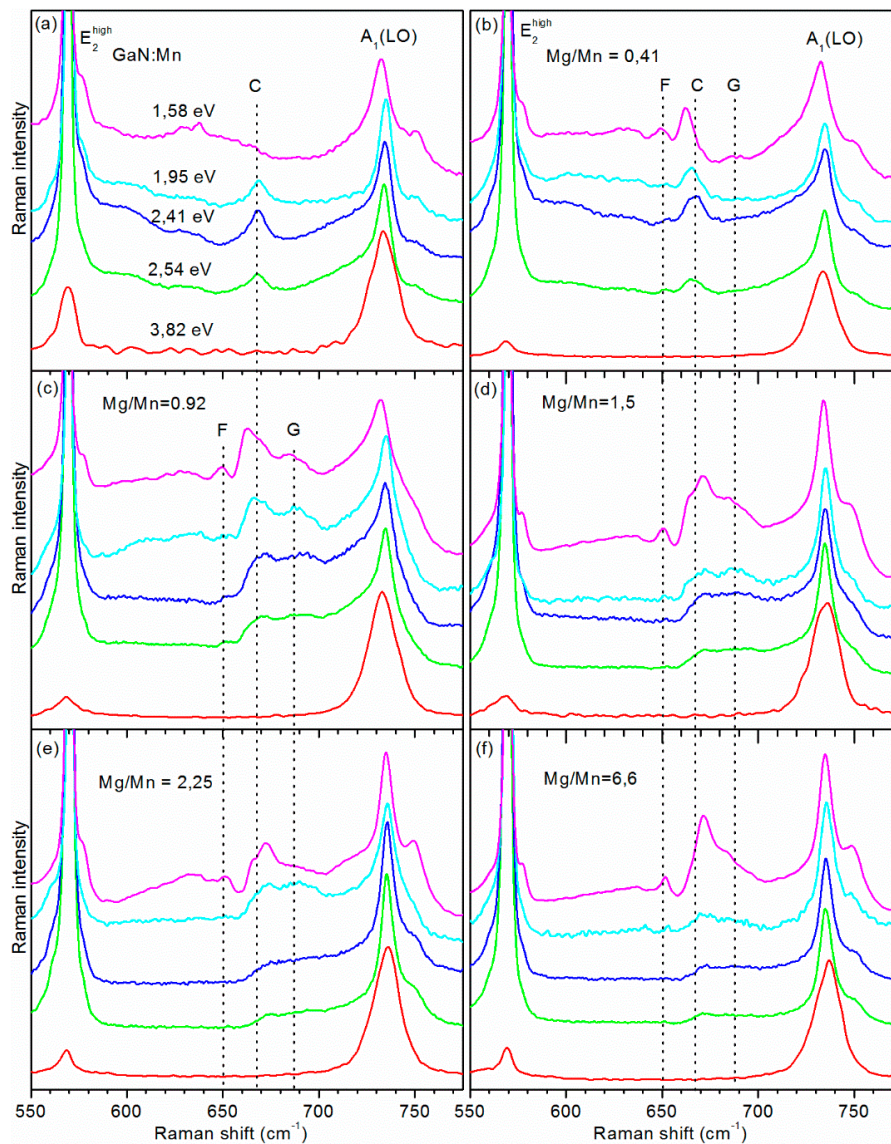


Figure 3. Resonance Raman spectra of GaN:Mn (a) and GaN:(Mn,Mg) as a function of the Mg/Mn ratio (b–f), measured at different energies of the laser excitation. The spectra are normalized to the intensity of the $A_1(\text{LO})$ mode of GaN.

The impurity-induced feature C is the main Raman resonance related to Mn. The intensity of this feature scales with the Mn concentration [8], thus in order to analyze its dependence on the excitation energy, as well as to compare the response of samples with different Mg/Mn ratios and Mn concentrations, its relative intensity with respect to the $A_1(\text{LO})$ mode of GaN is normalized to the corresponding intensity at the non-resonant excitation of 2.54 eV (Figure 4).

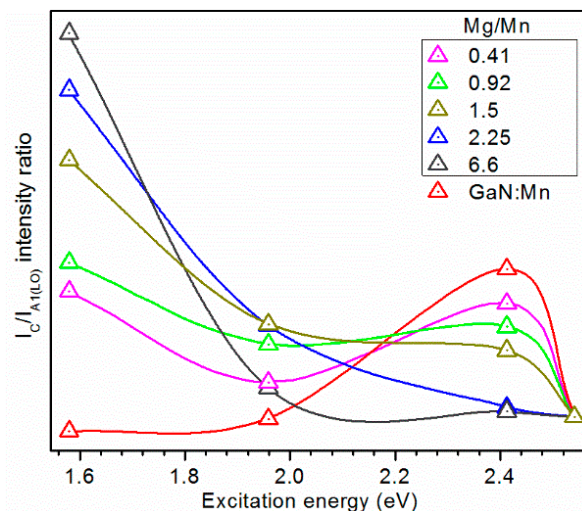


Figure 4. Integrated intensity of the Mn-induced feature C related to the $A_1(\text{LO})$ phonon mode of GaN as a function of the excitation energy and normalized to its intensity at 2.54 eV. Solid lines: guide for the eye.

The intensity of the Mn-induced mode C in GaN:Mn is the highest for an excitation energy of 2.41 eV, as evidenced in Figure 4. This resonance gradually weakens with increasing Mg/Mn ratio in the Mg co-doped samples, while a resonance at 1.58 eV is detected.

A detailed analysis of the Raman spectra at 1.58 eV suggests that the Mn-induced band C results from the convolution of two distinct components, denoted as C_1 and C_2 in Figure 5a. The relative intensity of these two contributions gradually changes upon varying the Mg/Mn ratio (Figure 5b), while their frequency gradually increases for $k \geq 2.25$ and then decreases for $k = 6.6$, similarly to the $A_1(\text{LO})$ mode of GaN (Figure 5c), but with an enhanced shift of the C_2 component. This frequency shift cannot be assigned to the effect of elastic strains solely, since the non-polar E_2^{high} mode, influenced by in-plane strain more significantly than the polar $A_1(\text{LO})$ mode [20], shows here a weak frequency dependence on the Mg/Mn ratio. The band at $(720\text{--}750)\text{ cm}^{-1}$ is a convolution of several phonon peaks with different origin: (i) a wide feature E, which—according to Gebicki et al. [9]—is related to disorder-induced scattering due to the activation of the phonon DOS; (ii) the $A_1(\text{LO})$ mode of GaN; (iii) a weak peak at 750 cm^{-1} originating from the sapphire substrate (the Raman spectrum of a reference bare sapphire substrate is shown in Figure 2a). The $A_1(\text{LO})$ mode is a single peak independent of the Mg/Mn ratio. The broad feature E does not show a significant dependence on the Mg/Mn ratio and gradually increases in intensity with the Mn content in the Mg co-doped samples, in [9] responding to local lattice disorder, which allows the observation of the phonon DOS.

The detected gradual increase in the relative intensity of the C_2 mode with the Mg/Mn ratio (Figure 5b) in general correlates with the increase of concentration of Mn-Mg_k complexes, in particular of Mn-Mg₂ and Mn-Mg₃ complexes in GaN:(Mn,Mg) samples [4]. According to [8], the peak position of the C_2 mode corresponds to the Mn-Mg₂ and Mn-Mg₃ complexes and correlates with their high Raman activity (the most significant contribution to Raman spectra). This is also in agreement with the population of different complexes, as calculated in [4]. Thus, the C_2 component can be ascribed to Mn-Mg₂ and Mn-Mg₃ complexes, while C_1 to the Mn-Mg₁ ones. The frequency of the C_2 component,

higher than that of C_1 , qualitatively agrees with the shortening of the Mn-N bond length in the presence of Mg [4].

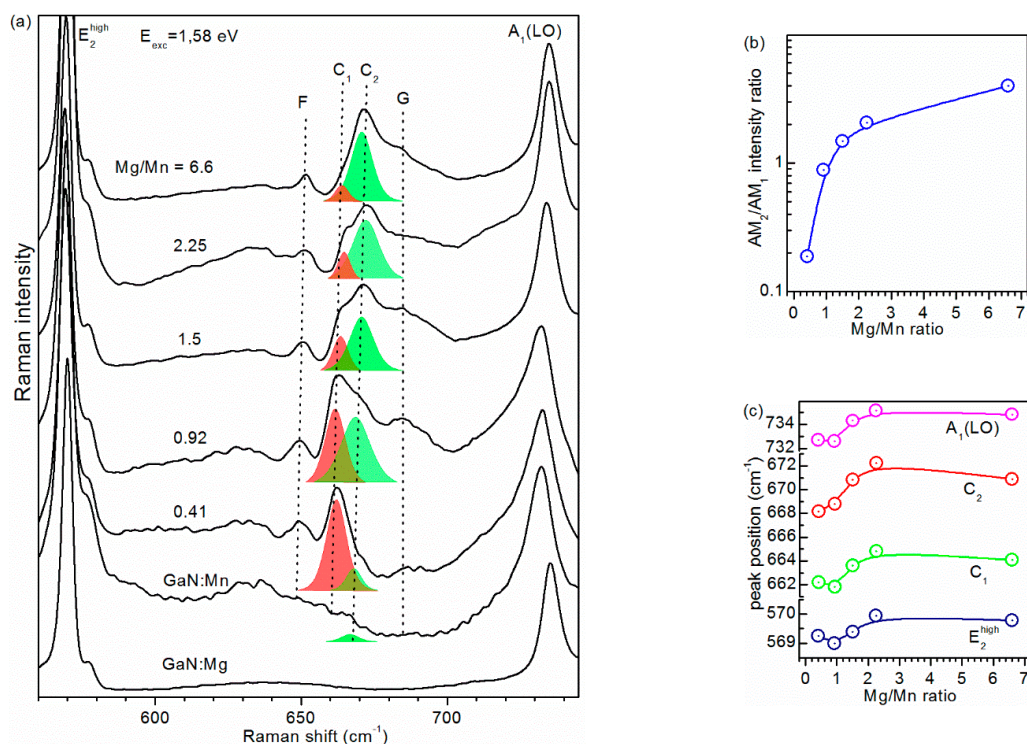


Figure 5. (a) Raman spectra of GaN:(Mn,Mg) at an excitation of 1.58 eV as a function of the Mg/Mn ratio. The relative intensity of the Mn-induced modes (b), indicated with C_1 and C_2 , and the peak positions of the different phonon modes (c) are given as a function of the Mg/Mn ratio.

The observed resonant behavior of the Mn-induced mode in GaN:(Mn,Mg) can be treated in the frame of a resonance Raman process similar to the one acting in GaN:Mn [9] and related to the charge transfer level of the Mn impurity, but additionally taking into account the changes in the Mn charge state due to the co-doping with Mg [4]. In GaN:Mn, Mn is mostly present in the neutral Mn^{3+} state with the $Mn^{3+/2+}$ acceptor level pinned at 1.8 eV above the valance band maximum of GaN, and the corresponding optical absorption resulting in the photoionization of neutral Mn [21]. However, in the co-doped samples, the presence of Mg alters the charge state of Mn, which is then found in the Mn^{5+} state [22]. Specifically, as reported in [23], the photoluminescence excitation (PLE) spectra of GaN:(Mn,Mg) show a broad band with an edge at 1.1 eV, assigned to electron excitation from the valance band of GaN to the Mn^{4+} level located at 1.1 eV above the top of the valance band. The broad band in the PLE spectra is caused by the presence of an absorption band, pointing at both hole photoionization and recombination. Therefore, considering the energy position of the Mn charge transfer level and applying the model proposed in [1], the enhancement of the Mn-induced Raman features in GaN:(Mn,Mg) at 1.58 eV is explained using impurity-induced one-LO-phonon resonance Raman scattering involving photoionization of a hole from the Mn donor level to the valance band and its subsequent recombination with ionized Mn^{4+} donors and with the emission of LO phonons.

In the case of Mn^{5+} ions (i.e., Mn-Mg₃ complexes) [22] the process of hole recombination after generation is hampered due to the positive charge state of Mn^{4+} with respect to the lattice. Therefore, the process results in a change of charge state from Mn^{5+} into Mn^{4+} , rather than in the capture of a hole by Mn^{4+} .

To probe the electron energy structure of the Mn impurity and to study the nature of the observed non-trivial enhancement of the Mn-induced phonon modes under sub-band excitation, PL spectroscopy was performed. The investigated GaN:(Mn,Mg) samples revealed two PL peaks at ~1.42 eV (Figure 6a)

and at ~ 1.05 eV (Figure 6b), respectively, with intensities which depend on the Mg/Mn ratio. The feature at ~ 1.42 eV is attributed to the 5T_2 - 5E intra-center transition of Mn^{3+} [24]. This PL line is most intense for GaN:Mn, and it gradually quenches with increasing Mg content (increase of the Mg/Mn ratio). The elusive intra-center photoluminescence of Mn^{3+} [21,24] is captured here, due to the specific resonant conditions of optical excitation close to the 5T_2 - 5E transition of Mn^{3+} . The PL peak at ~ 1.05 eV in GaN:Mn co-doped with Mg was shown to be related to internal transitions of the Mn^{5+} ion predominantly in the Mn-Mg₃ configuration [22].

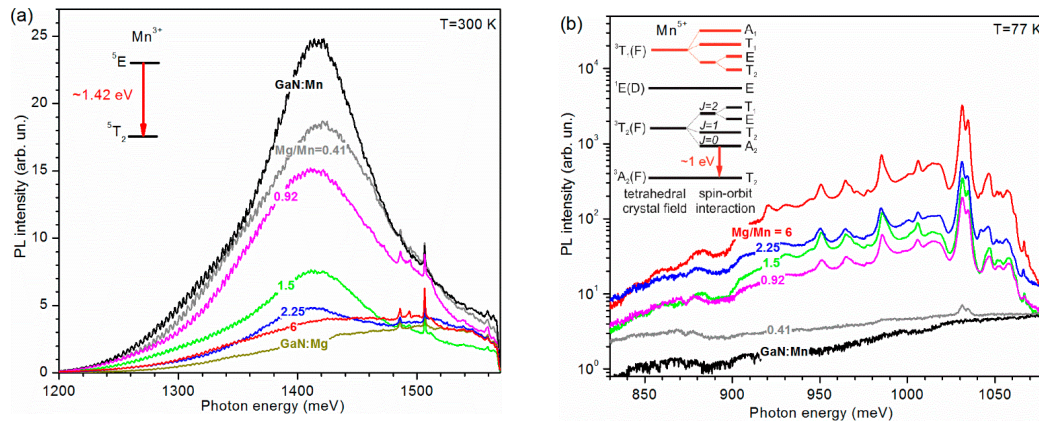


Figure 6. PL spectra from the GaN:(Mn,Mg) samples as a function of the Mg/Mn ratio measured (a) at an excitation of 1.58 eV at room temperature, and (b) at an excitation of 2.41 eV at $T = 77$ K. Insets to (a,b): term schemes of Mn^{3+} (a) and Mn^{5+} (b) in GaN.

Considering the energy position of the Mn charge transfer level, which in GaN:(Mn,Mg) is found to lie 1.1 eV above the top of the valence band of GaN, and applying the model proposed in [9], the enhancement of the Mn-induced Raman features in GaN:(Mn,Mg) at 1.58 eV is explained by impurity-induced one-LO-phonon resonance Raman scattering involving photoionization of a hole from the donor level of Mn to the valence band and its subsequent recombination with an ionized Mn^{5+} donor and with the emission of LO phonons. This impurity-induced resonance Raman process is efficient, due to the presence of the Mn-Mg_k cation complexes, favoring the energy transfer between a shallow Mg_{Ga} acceptor state and the Mn center, the capturing of the excited hole by the Mg acceptor, and its following transfer to the Mn center. The detected wide resonance energy profile of the Raman mechanism is also a fingerprint of the resonance process between the localized energy level and the band states.

3.2. Raman Spectroscopy at Inter-Band Excitation

The resonance Raman spectra for the GaN:(Mn,Mg) samples excited by an inter-band excitation of 3.82 eV are shown in Figure 7. The inter-band luminescence collected from the Mg-doped and undoped GaN significantly drops in intensity in the case of the Mn-doped samples, whereas multiphonon Raman scattering is detected. The first-order E_2^{high} and $A_1(LO)$ phonon peaks of GaN are well-resolved at 571 cm^{-1} and 735 cm^{-1} , respectively, and a strong resonance Raman scattering of the $A_1(LO)$ phonon is observed up to the seventh order. For excitation energies greater than the bandgap of GaN, the observed process is related to outgoing resonant Raman scattering (ORRS).

The intensity ratio between the overtone 2LO and the fundamental 1LO Raman bands makes it possible to evaluate the Huang-Rhys parameter S , which provides a measure of the strength of the electron-phonon interaction [25]. Specifically:

$$\left| \frac{I_{2LO}}{I_{1LO}} \right| = \frac{S}{2} \frac{(E_{ex} + \hbar\omega_{LO} - \hbar\omega_0)^2 + \Gamma^2}{(E_{ex} + 2\hbar\omega_{LO} - \hbar\omega_0)^2 + \Gamma^2}, \quad (1)$$

where the exciton energy E_{ex} is the difference between the energy bandgap E_g of GaN,—which depends on the Mn concentration [26]—and the exciton binding energy; Γ is the excitonic linewidth.

The dependence of the Huang-Rhys parameter S on the Mg/Mn ratio—estimated from the resonance Raman spectra in Figure 7—for the investigated GaN:(Mn,Mg) samples is shown in the inset to Figure 7. The Huang-Rhys parameter has a linear dependence on the Mg/Mn ratio, which points to an increment of the electron-phonon coupling strength. This result is consistent with theoretical *ab initio* calculations of spin density, which showed that complexing of Mn with one Mg tends to delocalize the spin density on the nitrogen atoms, while complexing with two or more Mg reduces the delocalization, thus enhancing the electron-phonon coupling [4].

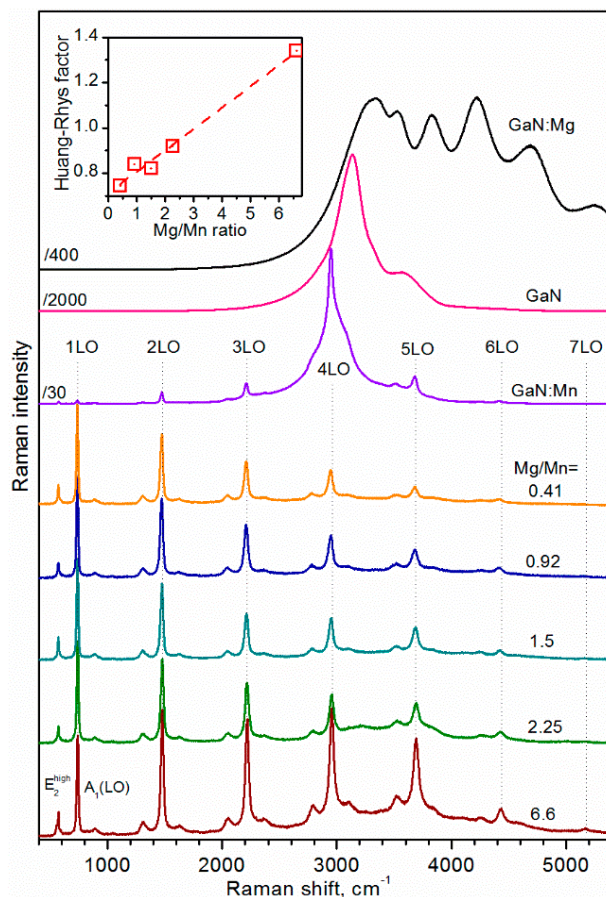


Figure 7. Resonance Raman spectra for the GaN:(Mn,Mg) samples measured at an inter-band excitation of 3.82 eV. Inset: dependence of the Huang-Rhys factor on the Mg/Mn.

The intensity of the multiphonon scattering is significantly dependent on the resonance condition of the ORRS process. The n -order LO-phonon peak increases in intensity up to the fourth order for GaN:Mn, where the 4LO peak is one order of magnitude higher than the 1LO. In contrast, for GaN:(Mn,Mg) this dependence is less pronounced and is superimposed to the general tendency of scattering peaks to decrease in intensity with the order n at a rate which depends on the Mg/Mn ratio.

The mechanism of ORRS acting here is pictured in the frame of the cascade model for exciton-mediated multiphonon resonant Raman scattering [27–29], whose schematic representation is shown in the inset to Figure 8. In this model the resonance features in the ORRS spectra are seen in the framework of a hot exciton cascade, and the scattering process is decomposed into sequential steps. In the first step, the incident photon ($E_{ex} = 3.185$ eV) is absorbed, an exciton is generated, and subsequently a LO phonon is emitted. In the second step, the exciton relaxes into lower energy states with the emission of LO phonons in a cascade process. In the third step, the exciton recombines radiatively, with the emission of a scattered photon ($\hbar\omega_s \approx \hbar\omega_0 - n\hbar\omega_{LO}$). Thus, the closer the exciton

energy E_{ex} and the difference between the excitation energy and n -order phonon mode are, the stronger the phonon mode is.

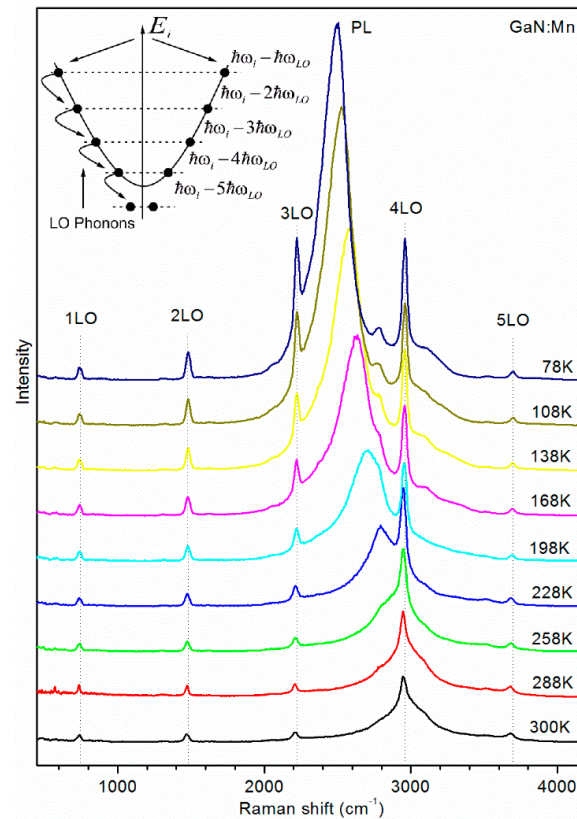


Figure 8. Resonance Raman spectra for the GaN:Mn sample measured at an inter-band excitation of 3.82 eV and in the temperature range (78–300) K. Inset: schematic diagram of the cascade model for the outgoing multiphonon resonant Raman scattering.

The behavior of multi-phonon Raman scattering, which is governed by the resonance with the band gap, can be tuned with temperature. The resonance Raman spectra of GaN:Mn at various temperatures in the range (78–300) K are shown in Figure 8. Besides causing a high-energy shift of the near-band edge (NBE) PL, the reduction of the temperature results in an enhancement of the multi-LO-phonon scattering, especially noticeable for the third and fourth order phonon scattering.

In the case of GaN:Mn the position of the NBE 3.511 eV PL peak at 77 K is about 30 meV lower than the position of the 3LO phonon peak and about 60 meV higher than the position of the 4LO peak. Considering the dependence of the $(\text{Ga}_{1-x}\text{Mn}_x)\text{N}$ band gap on the Mn concentration, i.e., $\Delta E_g = x(27.4 \pm 2.6)\text{meV}/\% - (0.89 \pm 1.13)\text{meV}$ [22], the GaN band gap $E_g^{\text{GaN}} = 3.507\text{ eV}$ at 77K, and the exciton binding energy of $E_x^A = 20.4\text{ meV}$ [30], the observed NBE PL is assigned to the recombination of free excitons in GaN:Mn. The observed high-energy shift of the excitonic PL peak at low temperatures (low-frequency Raman shift in Figure 8) is due to the temperature-induced widening of the band gap of GaN:Mn [31]. This effect is well described by the Varshni empirical formula and is consistent with the temperature dependence of the band-gap of pristine GaN [32]. The increase of temperature leads to the shift of the NBE PL to lower energies, due to the decrease in band gap energy, according to the Varshni empirical equation $E_g(T) = E_g(0) - \alpha T^2/(\beta + T)$ [27], where $\alpha = 8.32 \times 10^{-4}\text{ eV/K}$ and $\beta = 835.6\text{ K}$. The increase in energy difference between the 3LO peak and the exciton energy at the OMRRS conditions leads to the gradual weakening of this phonon mode with temperature (Figure 9a). For sample temperatures >200 K, the 4LO phonon mode undergoes a significant enhancement in intensity due to the proximity to the ORRS conditions, with a maximum enhancement at ~260 K.

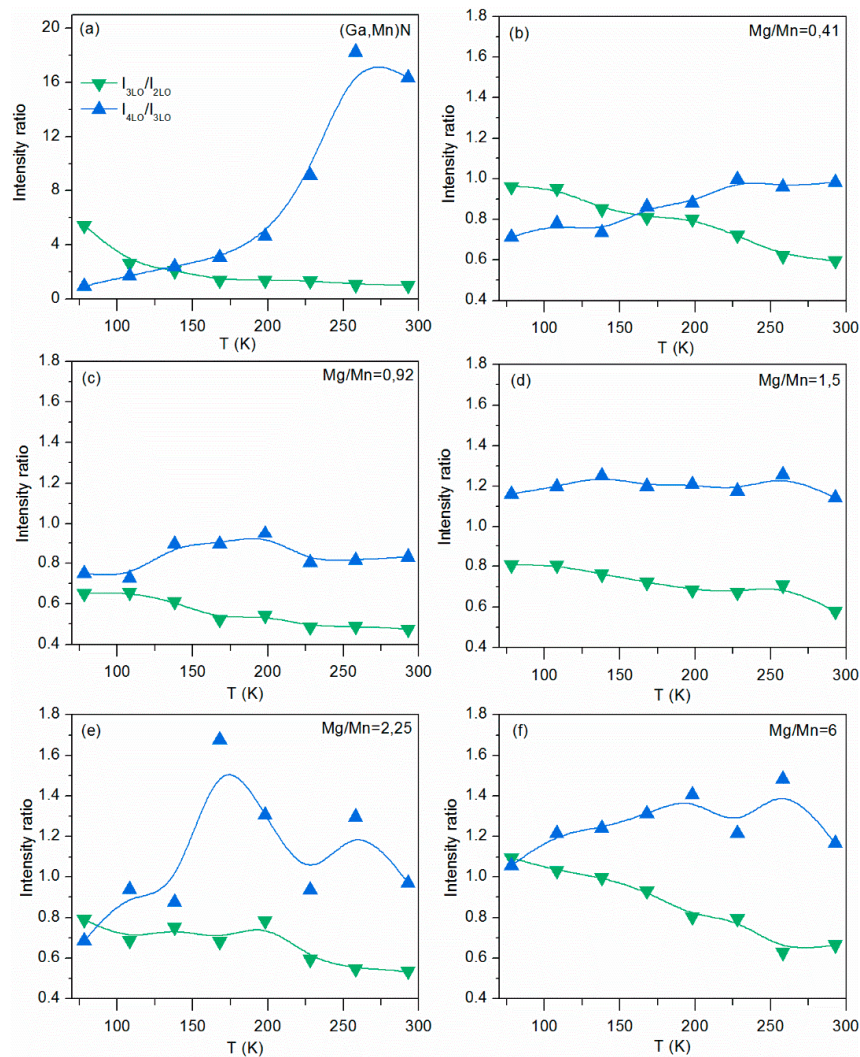


Figure 9. Temperature dependence of the I_{3LO}/I_{2LO} and I_{4LO}/I_{3LO} intensity ratios for GaN:Mn (a) and GaN:(Mn,Mg) with different Mg/Mn ratio (b–f).

The multi-phonon Raman scattering in GaN:(Mn,Mg) has shown a reduced dependence of the intensity of the 3LO and 4LO peaks on temperature, with significantly lower I_{3LO}/I_{2LO} and I_{4LO}/I_{3LO} relative intensities than those found for GaN:Mn (Figure 9b–f). The maxima in the temperature dependence of the I_{4LO}/I_{3LO} are less pronounced and shifted to lower temperature as compared to GaN:Mn. In particular, the maximum enhancement of the 4LO peak for GaN:(Mn,Mg) with Mg/Mn = 2.25 is observed at ~170 K, whereas its relative intensity I_{4LO}/I_{3LO} is over 10 times lower than that of GaN:Mn (Figure 9e). Within the ORRS conditions, the measured shift of the maximum intensity of the 4LO peak to lower temperatures is related to the interplay between the reduction in the bandgap of $(Ga_{1-x}Mn_x)N$ due to the lower Mn content in GaN:(Mn,Mg) and the temperature-induced widening of the bandgap. The lower intensity of the multiphonon peaks and the weaker resonant enhancement is related to the broadening of the band edges due to potential fluctuations induced by the high concentration of dopants [33]. The potential fluctuations which arise due to the inhomogeneous distribution of charged defects play a significant role in the optical properties of compensated or highly doped semiconductors. The broadening of the impurity bands in heavily doped semiconductors due to potential fluctuation can be described in the frame of the model proposed by Morgan et al. [34], which was successfully used to account for the broadening of NBE PL lines in GaN doped by Si [35]. On the other hand, a serious breakdown of the wave-vector conservation may occur in heavily doped semiconductors, due to scattering by random impurities. The relaxation of the quasi-momentum

conservation allows phonons with larger wave-vectors to participate in the Raman scattering, thus enhancing the intraband Fröhlich contribution and increasing the corresponding scattering cross section [33]. The correlation between the smearing of the band edges due to potential fluctuations and the mechanisms of resonant Raman scattering determines the temperature dependence of the multi-phonon LO peaks in the resonant Raman spectra. In addition, Mn-Mg_k cation complexes and defects can affect the ORRS enhancement through the inter-band Fröhlich mechanism and via exciton–impurity interaction [27–29,36,37].

4. Conclusions

Resonance Raman studies at room temperature of GaN:(Mn,Mg) have shown that in contrast to the case of GaN:Mn, the resonance enhancement of the Mn-induced modes in Mg co-doped samples is not observed at an excitation of 2.4 eV, but shifts to lower energies. This effect is explained by the resonance Raman process of photoionization of a hole from the donor level of Mn to the valence band of GaN, followed by the recombination with an ionized Mn⁵⁺ donor with the emission of LO phonons. Selective excitation within the resonance Raman conditions allows the structure of the main Mn-induced phonon band at ~670 cm^{−1} to be resolved into two distinct components, whose relative intensity varies with the Mg/Mn ratio, and can thus be related to the different Mn-Mg_k cation complexes. The enhancement of the Huang-Rhys factor at large Mg/Mn ratios reflects the increase of coupling strength of the electron-phonon interaction, in agreement with theoretical predictions. The selective enhancement of the 4LO phonon peak upon temperature reduction is due to the variation in resonance conditions of ORRS by detuning the band gap. The observed ORRS is explained via exciton-mediated multi-phonon Raman scattering and strong impurity-induced Fröhlich interaction. These findings contribute to the understanding of the vibrational properties and electron-phonon coupling of GaN:(Mn,Mg) with Mn-Mg_k cation complexes, relevant to gain insight into electron-phonon relaxation mechanisms, charge transport in this system [38–40], and their effect on the efficiency of prospective full-nitride IR emitters [22] and optically active and tunable spintronic devices [4,41].

Author Contributions: Conceptualization, A.N., V.S., D.K., and A.B.; investigation A.N., B.T., and G.C.; formal analysis, A.N. and B.T.; funding acquisition, V.S. and A.B.; writing—original draft, A.N. and B.T.; writing—review and editing, D.K. and A.B.

Funding: This work was supported by NATO SfP Grant 984735, by the State Fund for Fundamental Research project F83/72, and by the Austrian Science Foundation—FWF P26830 and P31423.

Acknowledgments: A. Nikolenko acknowledges Olena Fesenko for Raman measurements at 632 nm, Oleksii Ilchenko for Raman measurements at 785 nm, Nadiia Korsunskia and Roland Hayn for fruitful discussions.

Conflicts of Interest: The authors declare no conflict of interest.

References

1. Passow, T.; Gutt, R.; Kunzer, M.; Pletschen, W.; Kirste, L.; Forghani, K.; Scholz, F.; Köhler, K.; Wagner, J. High Power Efficiency AlGaIn-Based Ultraviolet Light-Emitting Diodes. *Jpn. J. Appl. Phys.* **2013**, *52*, 08JG16. [CrossRef]
2. Yoshida, H.; Yamashita, Y.; Kuwabara, M.; Kan, H. A 342-nm ultraviolet AlGaIn multiple-quantum-well laser diode. *Nat. Photonics* **2008**, *2*, 551–554. [CrossRef]
3. Amano, H.; Baines, Y.; Beam, E.; Borga, M.; Bouchet, T.; Chalker, P.R.; Charles, M.; Chen, K.J.; Chowdhury, N.; Chu, R.; et al. The 2018 GaN power electronics roadmap. *J. Phys. D. Appl. Phys.* **2018**, *51*, 163001. [CrossRef]
4. Devillers, T.; Rovezzi, M.; Szwacki, N.G.; Dobkowska, S.; Stefanowicz, W.; Sztankiel, D.; Grois, A.; Suffczyński, J.; Navarro-Quezada, A.; Faina, B.; et al. Manipulating Mn-Mg_k cation complexes to control the charge- and spin-state of Mn in GaN. *Sci. Rep.* **2012**, *2*, 722. [CrossRef] [PubMed]
5. Capuzzo, G.; Kysylychyn, D.; Adhikari, R.; Li, T.; Faina, B.; Tarazaga Martín-Luengo, A.; Bonanni, A. All-nitride Al_xGa_{1-x}N:Mn/GaN distributed Bragg reflectors for the near-infrared. *Sci. Rep.* **2017**, *7*, 42697. [CrossRef] [PubMed]

6. Wagner, J. Raman spectroscopy for impurity characterization in III-V semiconductors. *Appl. Surf. Sci.* **1991**, *50*, 79–86. [[CrossRef](#)]
7. *Semiconductor Research*; Patane, A.; Balkan, N. (Eds.) Springer Series in Materials Science; Springer: Berlin/Heidelberg, Germany, 2012; Volume 150, ISBN 978-3-642-23350-0. [[CrossRef](#)]
8. Devillers, T.; Leite, D.M.G.; Dias da Silva, J.H.; Bonanni, A. Functional Mn–Mg_k cation complexes in GaN featured by Raman spectroscopy. *Appl. Phys. Lett.* **2013**, *103*, 211909. [[CrossRef](#)]
9. Gebicki, W.; Dominik, P.; Podsiadlo, S. Lattice dynamics and Raman scattering from GaN:Mn crystals. *Phys. Rev. B* **2008**, *77*, 245213. [[CrossRef](#)]
10. Kaschner, A.; Siegle, H.; Kaczmarczyk, G.; Strassburg, M.; Hoffmann, A.; Thomsen, C.; Birkle, U.; Einfeldt, S.; Hommel, D. Local vibrational modes in Mg-doped GaN grown by molecular beam epitaxy. *Appl. Phys. Lett.* **1999**, *74*, 3281–3283. [[CrossRef](#)]
11. Harima, H.; Inoue, T.; Nakashima, S.; Ishida, M.; Taneya, M. Local vibrational modes as a probe of activation process in *p*-type GaN. *Appl. Phys. Lett.* **1999**, *75*, 1383–1385. [[CrossRef](#)]
12. Limmer, W.; Ritter, W.; Sauer, R.; Mensching, B.; Liu, C.; Rauschenbach, B. Raman scattering in ion-implanted GaN. *Appl. Phys. Lett.* **1998**, *72*, 2589–2591. [[CrossRef](#)]
13. Hasuike, N.; Fukumura, H.; Harima, H.; Kisoda, K.; Hashimoto, M.; Zhou, Y.K.; Asahi, H. Optical studies on GaN-based spintronics materials. *J. Physics-Condensed Matter* **2004**, *16*, S5811–S5814. [[CrossRef](#)]
14. Bonanni, A.; Sawicki, M.; Devillers, T.; Stefanowicz, W.; Faina, B.; Li, T.; Winkler, T.E.; Sztenkiel, D.; Navarro-Quezada, A.; Rovezzi, M.; et al. Experimental probing of exchange interactions between localized spins in the dilute magnetic insulator (Ga,Mn)N. *Phys. Rev. B Condens. Matter Mater. Phys.* **2011**, *84*, 1–11. [[CrossRef](#)]
15. Flack, T.J.; Pushpakaran, B.N.; Bayne, S.B. GaN Technology for Power Electronic Applications: A Review. *J. Electron. Mater.* **2016**, *45*, 2673–2682. [[CrossRef](#)]
16. Morkoc, H. *Handbook of Nitride Semiconductors and Devices*; Wiley-VCH Verlag GmbH & Co. KGaA: Weinheim, Germany, 2008; ISBN 9783527628438.
17. Lee, H.-P.; Perozek, J.; Rosario, L.D.; Bayram, C. Investigation of AlGaIn/GaN high electron mobility transistor structures on 200-mm silicon (111) substrates employing different buffer layer configurations. *Sci. Rep.* **2016**, *6*, 37588. [[CrossRef](#)] [[PubMed](#)]
18. Ilchenko, O.; Pilgun, Y.; Makhnii, T.; Slipets, R.; Reynt, A.; Kutsyk, A.; Slobodianiuk, D.; Koliada, A.; Krasnenkov, D.; Kukharsky, V. High-speed line-focus Raman microscopy with spectral decomposition of mouse skin. *Vib. Spectrosc.* **2016**, *83*, 180–190. [[CrossRef](#)]
19. Dias da Silva, J.H.; Leite, D.M.G.; Zanatta, A.R. Resonant excitation of Mn local vibrational modes in the higher order Raman spectra of nanocrystalline Ga_{1-x}Mn_xN films. *J. Phys. Condens. Matter* **2008**, *20*, 252201. [[CrossRef](#)]
20. Demangeot, F.; Frandon, J.; Renucci, M.A.; Briot, O.; Gil, B.; Aulombard, R.L. Raman determination of phonon deformation potentials in α -GaN. *Solid State Commun.* **1996**, *100*, 207–210. [[CrossRef](#)]
21. Graf, T.; Gjukic, M.; Brandt, M.S.; Stutzmann, M.; Ambacher, O. The Mn^{3+/2+} acceptor level in group III nitrides. *Appl. Phys. Lett.* **2002**, *81*, 5159–5161. [[CrossRef](#)]
22. Kysylychyn, D.; Suffczyński, J.; Woźniak, T.; Gonzalez Szwacki, N.; Bonanni, A. Resonant excitation of infrared emission in GaN:(Mn,Mg). *Phys. Rev. B* **2018**, *97*, 245311. [[CrossRef](#)]
23. Han, B.; Wessels, B.W.; Ulmer, M.P. Optical investigation of electronic states of Mn⁴⁺ ions in *p*-type GaN. *Appl. Phys. Lett.* **2005**, *86*, 1–4. [[CrossRef](#)]
24. Zenneck, J.; Niermann, T.; Mai, D.; Roever, M.; Kocan, M.; Malindretos, J.; Seibt, M.; Rizzi, A.; Kaluza, N.; Hardtdegen, H. Intra-atomic photoluminescence at 1.41 eV of substitutional Mn in GaMnN of high optical quality. *J. Appl. Phys.* **2007**, *101*, 2005–2008. [[CrossRef](#)]
25. Zhang, Q.; Zhang, J.; Utama, M.I.B.; Peng, B.; De La Mata, M.; Arbiol, J.; Xiong, Q. Exciton-phonon coupling in individual ZnTe nanorods studied by resonant Raman spectroscopy. *Phys. Rev. B Condens. Matter Mater. Phys.* **2012**, *85*, 1–9. [[CrossRef](#)]
26. Suffczyński, J.; Grois, A.; Pacuski, W.; Golnik, A.; Gaj, J.A.; Navarro-Quezada, A.; Faina, B.; Devillers, T.; Bonanni, A. Effects of *s,p*-*d* and *s*-*p* exchange interactions probed by exciton magnetospectroscopy in (Ga,Mn)N. *Phys. Rev. B Condens. Matter Mater. Phys.* **2011**, *83*, 1–8. [[CrossRef](#)]
27. Martin, R.M.; Varma, C.M. Cascade Theory of Inelastic Scattering of Light. *Phys. Rev. Lett.* **1971**, *26*, 1241–1244. [[CrossRef](#)]

28. Sun, W.H.; Chua, S.J.; Wang, L.S.; Zhang, X.H. Outgoing multiphonon resonant Raman scattering and luminescence in Be- and C-implanted GaN. *J. Appl. Phys.* **2002**, *91*, 4917–4921. [[CrossRef](#)]
29. Kaschner, A.; Hoffmann, A.; Thomsen, C. Resonant Raman scattering on free and bound excitons in GaN. *Phys. Rev. B Condens. Matter Mater. Phys.* **2001**, *64*, 1–7. [[CrossRef](#)]
30. Muth, J.F.; Lee, J.H.; Shmagin, I.K.; Kolbas, R.M.; Casey, H.C.; Keller, B.P.; Mishra, U.K.; DenBaars, S.P. Absorption coefficient, energy gap, exciton binding energy, and recombination lifetime of GaN obtained from transmission measurements. *Appl. Phys. Lett.* **1997**, *71*, 2572–2574. [[CrossRef](#)]
31. Guo, L.L.; Shen, W.Z.; Zhang, Y.H. Temperature dependence of the optical properties in GaMnN. *J. Appl. Phys.* **2006**, *99*, 113533. [[CrossRef](#)]
32. Shan, W.; Schmidt, T.J.; Yang, X.H.; Hwang, S.J.; Song, J.J.; Goldenberg, B. Temperature dependence of interband transitions in GaN grown by metalorganic chemical vapor deposition. *Appl. Phys. Lett.* **1995**, *66*, 985–987. [[CrossRef](#)]
33. Ursaki, V.V.; Tiginyanu, I.M.; Zalamai, V.V.; Rusu, E.V.; Emelchenko, G.A.; Masalov, V.M.; Samarov, E.N. Multiphonon resonant Raman scattering in ZnO crystals and nanostructured layers. *Phys. Rev. B Condens. Matter Mater. Phys.* **2004**, *70*, 1–8. [[CrossRef](#)]
34. Morgan, T.N. Broadening of Impurity Bands in Heavily Doped Semiconductors. *Phys. Rev.* **1965**, *139*, A343–A348. [[CrossRef](#)]
35. Iliopoulos, E.; Doppalapudi, D.; Ng, H.M.; Moustakas, T.D. Broadening of near-band-gap photoluminescence in n-GaN films. *Appl. Phys. Lett.* **1998**, *73*, 375–377. [[CrossRef](#)]
36. García-Cristbal, A.; Cantarero, A.; Trallero-Giner, C.; Cardona, M. Excitonic model for second-order resonant Raman scattering. *Phys. Rev. B* **1994**, *49*, 13430–13445. [[CrossRef](#)]
37. Martin, R.M. Resonance raman scattering near critical points. *Phys. Rev. B* **1974**, *10*, 2620–2631. [[CrossRef](#)]
38. Jhalani, V.A.; Zhou, J.-J.; Bernardi, M. Ultrafast Hot Carrier Dynamics in GaN and Its Impact on the Efficiency Droop. *Nano Lett.* **2017**, *17*, 5012–5019. [[CrossRef](#)] [[PubMed](#)]
39. Zhukov, V.P.; Tyuterev, V.G.; Chulkov, E.V.; Echenique, P.M. Electron-phonon relaxation and excited electron distribution in gallium nitride. *J. Appl. Phys.* **2016**, *120*, 085708. [[CrossRef](#)]
40. Wang, K.; Simon, J.; Goel, N.; Jena, D. Optical study of hot electron transport in GaN: Signatures of the hot-phonon effect. *Appl. Phys. Lett.* **2006**, *88*, 1–3. [[CrossRef](#)]
41. Smoleński, T.; Kazimierczuk, T.; Kobak, J.; Goryca, M.; Golnik, A.; Kossacki, P.; Pacuski, W. Magnetic ground state of an individual Fe²⁺ ion in strained semiconductor nanostructure. *Nat. Commun.* **2016**, *7*, 1–7. [[CrossRef](#)] [[PubMed](#)]



© 2019 by the authors. Licensee MDPI, Basel, Switzerland. This article is an open access article distributed under the terms and conditions of the Creative Commons Attribution (CC BY) license (<http://creativecommons.org/licenses/by/4.0/>).